ELSEVIER

Journal of Nuclear Materials 274 (1999) 273–286

journal of nuclear materials

www.elsevier.nl/locate/jnucmat

Annealing behaviour of reactor pressure-vessel steels studied by positron-annihilation spectroscopy, Mössbauer spectroscopy and transmission electron microscopy

V. Slugeň [a,*], D. Segers [b], P.M.A. de Bakker [c], E. De Grave [b], V. Magula [d], T. Van Hoecke [b], B. Van Waeyenberge [b]

[a] *Department of Nuclear Physics and Technology, FEI STU Bratislava, Ilkovičova 3, 812 19 Bratislava, Slovak Republic*
[b] *Department of Subatomic and Radiation Physics, RUG, Proeftuinstraat 86, B-9000 Gent, Belgium*
[c] *SCK-CEN, Reactor Materials Research Unit, Boeretang 200, 2400 Mol, Belgium*
[d] *Welding Research Institute, Račianska 71, Bratislava, Slovak Republic*

Received 18 May 1998; accepted 26 February 1999

Abstract

The annealing behaviour of commonly used reactor pressure-vessel steels was studied using positron-annihilation spectroscopy (PAS) (lifetime and Doppler broadening techniques), transmission Mössbauer spectroscopy (MS), integral low-energy electron MS (ILEEMS) and transmission electron microscopy (TEM). The results of these methods applied to different types of steels are discussed. Some significant differences in the experimental results are observed between the Russian (3 types) and Western Europe (5 types) steels and between individual specimens within these two groups. All specimens were annealed in vacuum and studied after this thermal treatment. It was confirmed that the heat affected zone (HAZ) is the most sensitive region for thermal and neutron irradiation-induced embrittlement in the reactor. Positron-annihilation lifetime measurements on HAZ specimens annealed at successively higher temperatures show the drastic increase in the vacancy-type defect formation between 525°C and 600°C. Therefore these specimens were selected for further detailed studies by TEM.

1. Introduction

One of the most fundamental tasks of nuclear-reactor safety research is assessing the integrity of the reactor pressure vessel (RPV). The properties of RPV steels and the influence of thermal and neutron treatment on these properties are routinely investigated by macroscopic methods such as Charpy V-notch and tensile tests. It turns out that the embrittlement of steel is a very complicated process depending on many factors (thermal and radiation treatment, chemical compositions, preparing conditions, ageing, etc). A number of semi-empirical laws, based on macroscopic data, have been established but unfortunately, these laws are never completely consistent with all data and do not provide the desired accuracy. Therefore, many additional test methods [1] have been developed to unravel the complex microscopic mechanisms responsible for RPV steel embrittlement.

The present study is based mainly on experimental data of positron-annihilation spectroscopy (PAS) and Mössbauer spectroscopy (MS) obtained from measurements on eight different types of RPV steels used in eastern as well as in western nuclear-power plants (NPP), and from transmission electron microscopy (TEM) on the Russian RPV steels 15Kh2MFA and 15Kh2NMFA.

RPV embrittlement is a more pronounced problem in eastern (Russian) types of nuclear reactors (VVER-440). It is due to the narrower gap between the outside surface of the core barrel and the inside surface of the RPV as compared to western RPVs.

* Corresponding author. Tel.: +421-7 6542 7207; fax: +421-7 6542 7207; e-mail: slugen@elf.stuba.sk

0022-3115/99/$ – see front matter
PII: S0022-3115(99)00073-2

The relatively small diameter ($\Phi_{in} = 3542$ mm in case of VVER-440/V-230 type) facilitates transport and installation of the RPV, but, on the other hand, the neutron fluxes and consequently neutron fluences on the RPV wall is generally higher than in other equivalent types. This influence of neutron flux (even neutrons of energy over 0.1 MeV) on RPV embrittlement is much more impressive than contributions from a coolant temperature or an operational pressure in the primary circuit.

Since the mid 1980s, PAS has been frequently used for examining RPV steels [2–4]. The positron-annihilation techniques (lifetime, Doppler broadening and ACAR measurements) can give essential information about the deterioration of the mechanical properties of RPV steels (matrix defects, precipitates) during irradiation, which is known as neutron embrittlement. The positron-lifetime technique is a well-established method for studying open-volume-type atomic defects and defect-impurity interactions in metals [5,6]. The lifetime of positrons trapped at radiation-induced vacancies, vacancy–impurity pairs, dislocations, microvoids, etc. is longer than that of free positrons in an undisturbed region in the same material. As a result of the presence of open-volume defects, the average positron lifetime observed in structural materials is found to increase with radiation damage. However, in more complex systems like steels, various atomic defects, vacancies, vacancy clusters, vacancy–impurity complexes, dislocations, precipitates, misfits on the grain boundaries, etc., coexist, and the interpretation of the experimental results is neither easy nor straightforward [1,7].

According to previous reports [3,4] it seems to be generally accepted that even in the western types of RPV steels containing more than 0.1 wt% of Cu, the Cu- and P-rich precipitates play a dominant role in thermal and neutron embrittlement. In case of eastern-type RPV steels, comprehensive PAS studies [2,8–10] have suggested that carbide formation is an important additional microstructural mechanism.

TEM provides essential information about the strain field of small precipitates and defect clusters. Number density, size and structure of features with diameter above the visibility limit of 2 nm are detectable in TEM. The secondary hardening and precipitation kinetics can also be observed and analysed using this technique. Therefore, the application of TEM is in many respects very useful in steel investigations.

MS is a powerful analytical technique because of its specificity for one single element and because of its extremely high sensitivity to changes in the atomic configuration in the near vicinity of the probe isotopes (in this case ^{57}Fe). MS measures hyperfine interactions and these provide valuable and often unique information about the magnetic and electronic state of the iron species, their chemical bonding to co-ordinating ligands, the local crystal symmetry at the iron sites, structural defects, lattice-dynamical properties, elastic stresses, etc. [11,12]. In general, a Mössbauer spectrum shows different components if the probe atoms are located at lattice positions, which are chemically unequivalent. From the parameters that characterise a particular Mössbauer sub-spectrum it can, for instance, be established whether the corresponding probe atoms reside in sites which are not affected by structural lattice defects, or whether they are located at defect-correlated positions. In this respect, however, it is almost imperative to combine Mössbauer measurements with other research methods, which preferably are sensitive to the nature of the defect properties. Combining the results of MS with those of TEM and PAS (and possibly of various other techniques [13]) on the same samples seems to be a promising approach, and hence efforts in that respect are recommended since they may be of significant technological importance for future developments of nuclear-reactor elements which are likely to be exposed to severe radiation damage.

2. Lifetime PAS study of RPV-steels

2.1. Experimental

In total eight non-irradiated specimens from different commonly used RPV steels were studied using PAS lifetime technique since 1996. JRQ and EGF are Japanese and German ferric steels, often used as the reference base metal in the construction of western nuclear reactors. The sample 73W is an American Linde 0124 weld metal. Beside these, two surveillance specimen base materials from Belgian NPP Doel (D4) and Chooz (CH) were studied. With the aim to compare western types of RPV steels to eastern types, 15Kh2MFA (specimens YA and YTA) and 15Kh2NMFA (XTA) RPV steels were measured as well. This Russian second-generation Cr–Mo–V type of RPV steel has been commercially used in VVER-440 and VVER-1000 nuclear reactors built also in the central and Eastern Europe countries since the 1970s. Specimens XTA and YTA were prepared in laboratory conditions as the proper simulation (coarse grain area) of the heat-affected zone (HAZ) of welded joint ($T_{max} = 1300$°C, $\Delta t_{8/5} = 30$ s). Thermorestor equipment was used for the proper simulation of welding thermocycle. The suggestion of heat treatment parameters (temperature level and dwell time) followed from the basic knowledge about the problems of reheat and underclad cracks [14].

The key elements in the chemical composition of the RPV steel specimens are given in Table 1. All of used PAS specimens were prepared by grinding small disks ($\varnothing = 5$ mm; initial thickness approx. 1 mm) to a thickness of about 0.3 mm. Final polishing was performed using

Table 1
Chemical composition of the studied RPV steel specimens

Code	Type of steel	Contents of alloying elements in RPV specimens (wt%)											
		C	Si	Mn	Mo	Ni	Cr	Cu	P	S	V	Co	Total
EGF	22NiMoCr37	0.22	0.23	0.88	0.51	0.84	0.39	0.080	0.006	0.004			3.160
D4	A508B Cl.3	0.20	0.28	1.43	0.53	0.75	–	0.055	0.008	0.008			3.261
CH	18MND5	0.18	0.26	1.55	0.50	0.65	0.18	0.140	0.007	0.002			3.469
JRQ	A533B Cl.	0.18	0.24	1.42	0.51	0.84	0.14	0.140	0.017	0.004			3.491
73W (weld)	Linde 0124	0.10	0.45	1.56	0.58	0.60	0.25	0.310	0.005	0.005			3.860
YA	15Kh2MFA	0.14	0.31	0.37	0.58	0.2	2.64	0.090	0.014	0.017	0.27	0.019	4.650
YTA (HAZ)	15Kh2MFA	0.14	0.24	0.40	0.72	0.14	2.93	0.110	0.013	0.017	0.31	0.011	5.031
XTA (HAZ)	15Kh2NMFA	0.18	0.24	0.52	0.62	1.26	2.22	0.080	0.010	0.013	0.08	0.008	5.231

diamond paste with grains of about 1 μm. No dependence on the specimen preparation was found in comparative measurements.

The annealing behaviour of the specimens was studied with isochronal annealing of 30 min duration between room temperature (RT) and 700°C. Temperature steps of 50°C and 25°C in the most interesting region were chosen. The treatments were performed in vacuum better than 3×10^{-3} Pa. The cooling speed was slower than 100°C/h.

The positron lifetime spectra were measured at RT with a conventional fast–fast timing system. The resolution of the apparatus was about 300 ps FWHM for 511–1274 keV gamma-coincidences. The ^{22}Na positron source with an activity of about 36 μCi was fixed between 7.5 μm thick kapton foils and sandwiched between the specimen disks. At least 4×10^6 counts in the whole spectrum were collected for each studied specimen.

The Doppler broadening measurements were performed using a germanium detector with an energy resolution of 1.2 keV at 511 keV.

2.2. Results and discussion to PAS lifetime measurements

Several types of analyses and fitting approaches have been performed on the measured data. The optimum decomposition of lifetimes and the proper physical model for interpretation was searched using the reasonable combination of programs POSITRONFIT [15] and MELT [16]. From the lifetime distributions (MELT) analyses, it was clear that the spectra are so complicated, that beside the source (kapton) corrections only one or two components as a maximum, could be seriously considered.

Therefore, we performed a source correction by fixing not only the lifetime of the kapton ($\tau_K = 382$ ps) but also its intensity ($I_K = 13.5\%$). This approach was taken according to our extensive MELT analyses, supported also by works [17,18] describing the proper kapton correction by low-alloyed steels measurement. We neglected the long-lifetime component at the average value of about $\tau_{LT} = 1500$ ps and $I_{LT} = 0.3\%$. Its presence can be explained as a contribution from a thin surface oxide layer [8] and was almost constant.

Due to the very complicated defect structure in the studied steels, first we analysed all the spectra with only one mean lifetime. Comparisons of the results for all studied RPV steel specimens are given in Figs. 1 and 2.

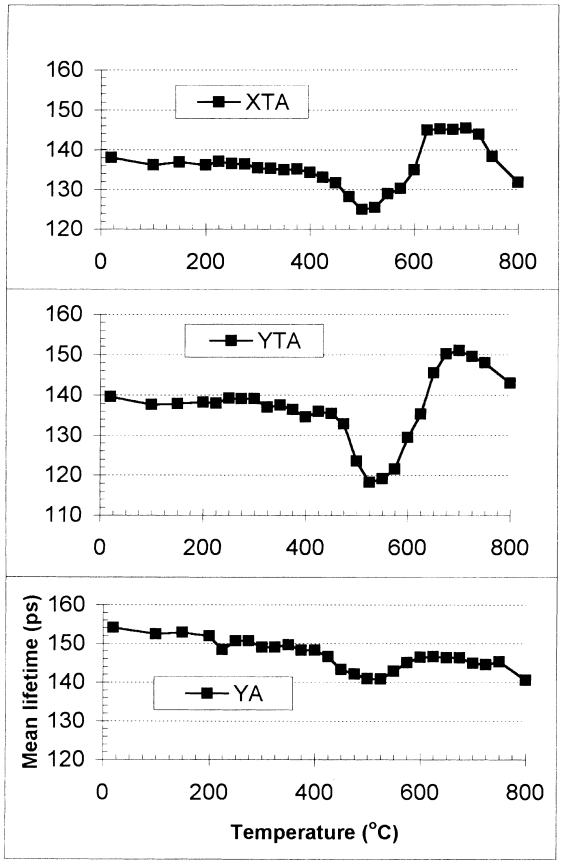

Fig. 1. Evolution of the mean positron lifetime for Russian-type RPV steels after suitable source correction. Specimens YTA and YA are from 15Kh2MFA steel, specimen XTA is from 15Kh2NMFA steel.

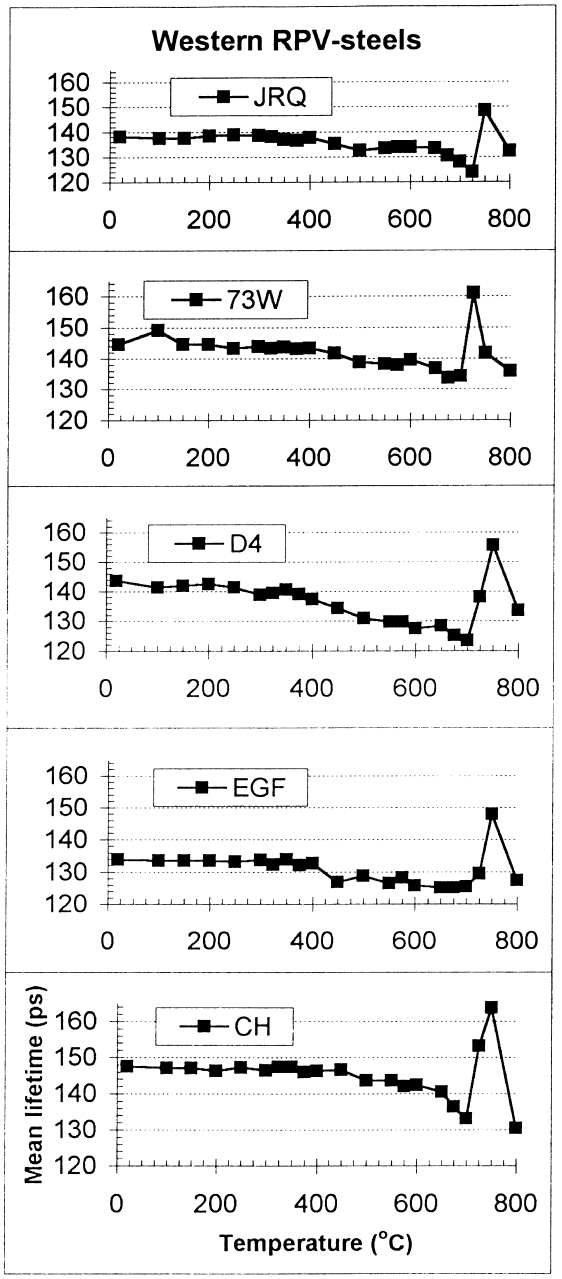

Fig. 2. Evolution of the mean positron lifetime for western-type RPV steels after suitable source correction.

At the first glance there are significant differences between western and Russian types of steels, but also between individual specimens within these two groups. The mean lifetime in Russian steels is more sensitive to temperature changes (up to 15%, see Fig. 1). After the minima the mean lifetime increases, in case of XTA and YTA specimens to significant higher values than the initial ones. It is caused due to different heat treatment parameters (temperature level and the dwell time) because the samples YA and YTA have the same chemical composition. Both specimens simulated HAZ (XTA and YTA) were studied in the most interesting region (500–720°C) using TEM more in detail (see ch. 5).

For western steels (JRQ, 73W, EGF and CH), the mean lifetimes decrease more slowly (up to ~5–6%, if we neglect the probable artefact at 100°C in the case of 73W specimen). Only for specimen D4 the lowering is more pronounced (≃10%). The minima are shallower than those for the Russian steels.

The two component analysis results are shown in Figs. 3 and 4. In case of the Russian 15Kh2MFA and 15Kh2NMFA steels, the lifetime values are relatively stable at about $\tau_1 = 70$ ps and $\tau_2 = 150$ ps. The significant change observed at YTA steel in the mean lifetime study was confirmed also here in the rapid increase of τ_2. The maximum was reached at about 525°C, and hints at the new cluster formation of vacancies, which are removed by further heat treatment. No 'jumps' of τ_2 values were observed at 725°C. Changes in steels due to the starting phase transition from bcc to fcc were observed on all western-types of RPV-steels. The same phenomenon appeared also in case of MS, when the presence of the paramagnetic austenite was clearly detected at 750°C in western batches of steels and at 800–850°C in Russians steels.

The lifetime curves of the two-component analyses, performed at western types of RPV steel, are slightly different. Except the already mentioned increase at 725°C, the major differences are observable in the trendlines of the shorter τ_1 lifetimes. After decrease of τ_1 values (well-detected especially at JRQ, 73W and D4 specimens) an increase at about 350°C was measured almost at all types of western steels. These changes of τ_1 values are not detectable in Russian RPV steels. The levels of the longer lifetime component τ_2 are in the temperature region up to 700°C almost constant ($\tau_2 = 150$ ps) and are comparable with Russian YA and XTA steels. In case of 73W specimen the τ_2 is higher (successive increase up to 250 ps).

Many trials were undertaken on the three-component analyses. The POSITRONFIT results obtained with this approach to the mathematical decomposition of the spectra in three different lifetime components were not always possible or satisfactory.

2.3. Results from Doppler broadening measurements

In addition to positron lifetime measurements, we started also with Doppler broadening measurements on two Russian 15Kh2MFA and 15Kh2NMFA RPV steels. Specimens were prepared and treated in the same way as in case of positron lifetime measurements. *S*-parameter measurements were done to get an idea of what effects can be observed using this method and if

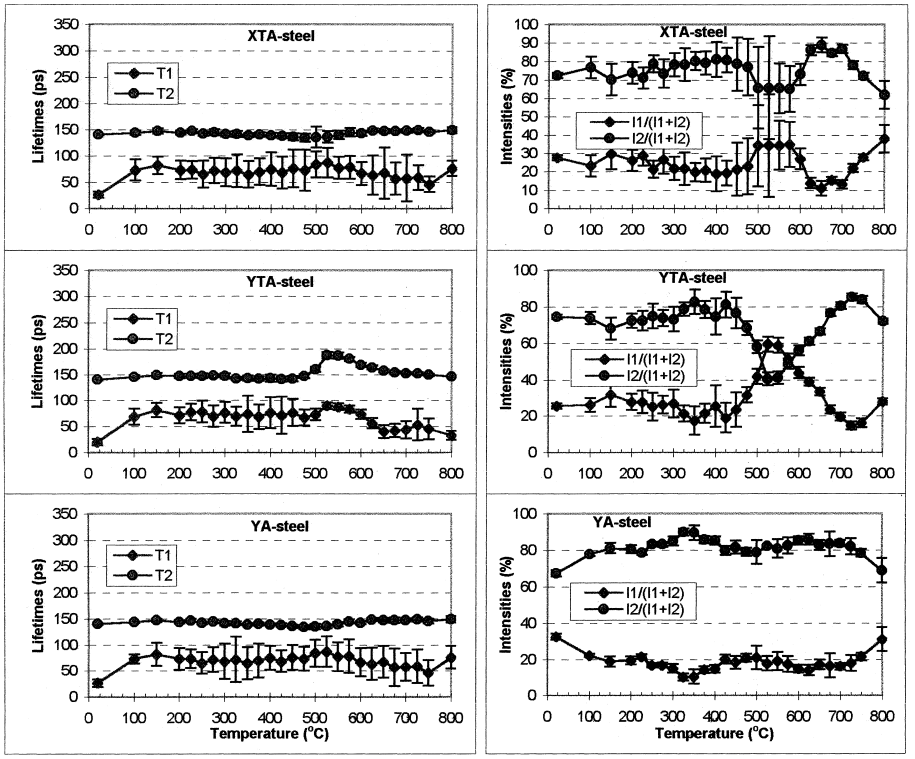

Fig. 3. The two-components analysis of Russian RPV-steel specimens.

this type of measurement gives some additional information to the results obtained using the PAS lifetime technique.

The results of the Doppler broadening parameter S as a function of successive isochronal annealing (30 min) at different temperatures for the Russian RPV steels 15Kh2MFA and 15Kh2NMFA are shown in Fig. 5. The calibration constant was held in each case on 0.0468 and the statistical error better than 0.04%.

In the case of both types of steels our results confirm changes in the electron momentum distribution due to thermal treatment. The maximum is observable at about 500°C. This fact is in agreement with results from PAS lifetime measurements, from which the electron concentration can be evaluated. More efficiency of Doppler broadening measurements is expected in case of irradiated specimens.

3. Mössbauer spectroscopy

3.1. Comparison between different types of non-irradiated RPV-steel specimens from the MS point of view

Mössbauer spectra for different non-irradiated RPV steel specimens have been recorded at RT in transmission geometry using a constant-acceleration drive with triangular source motion. The absorbers were prepared by polishing small disks (initial thickness approximately 1 mm) to a thickness of 50 μm or less. Spectra were run until an off-resonance count rate of at least 1×10^6 for the unfolded spectrum was reached. The spectrometer was calibrated with respect to natural iron. All quoted isomer shifts δ are relative to α-Fe.

Differences between Mössbauer spectra obtained from different eastern as well as western types of RPV-steels (see Table 1) were already discussed in detail [19]. Our current MS measurements were focused mainly on the isochronal annealing of RPV-steels and comparison between irradiated and non-irradiated specimens after annealing processes.

3.2. Isochronal annealing of RPV-steels, comparison between irradiated and non-irradiated specimens from the MS point of view in laboratory conditions

A total of seven specimens from four different, commonly used RPV steels were selected for this study: JRQ and HSST03 are A533B Cl. 1 steels that often serve as base metal in the construction of western nuclear reactors. From both materials irradiated as well as non-irradiated specimens were annealed (JRQ616, X51:

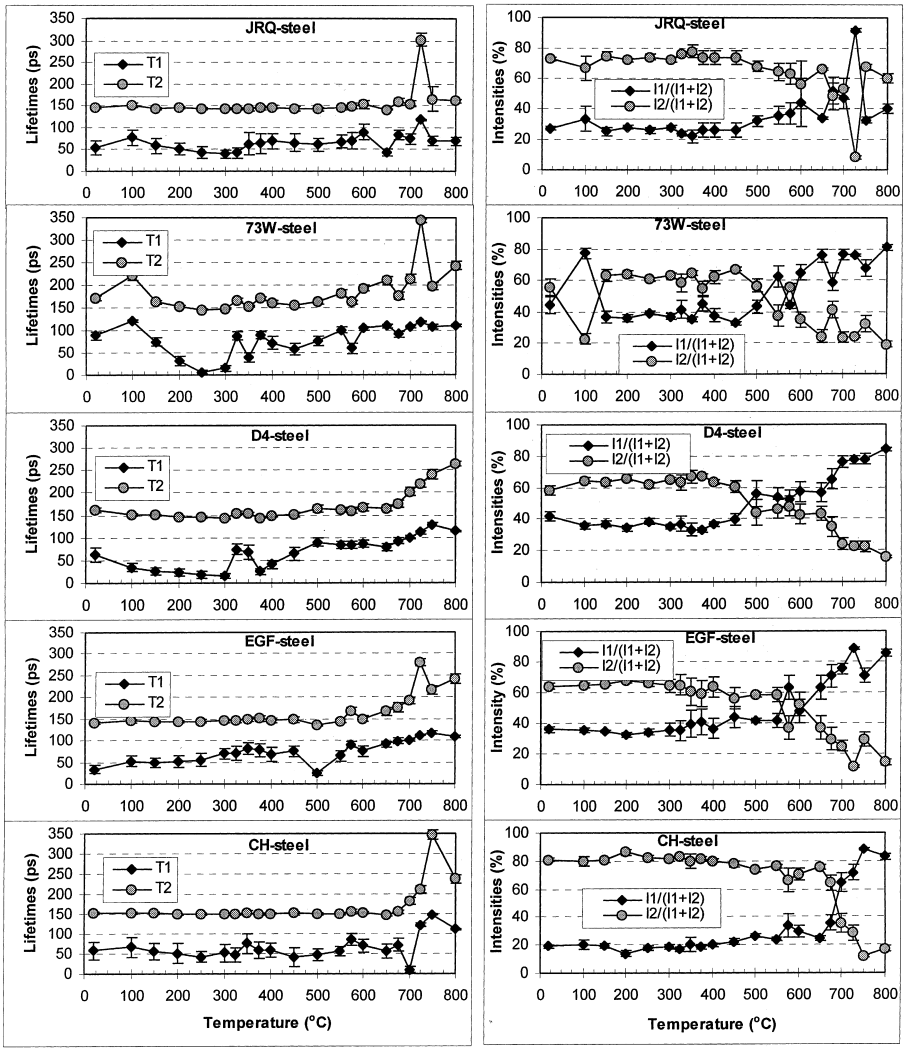

Fig. 4. The two-components analysis of western RPV-steel specimens.

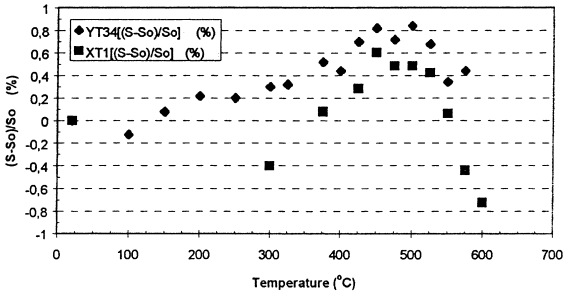

Fig. 5. Results of the Doppler broadening parameter S in form of $(S-S_0)/S_0$ as a function of successive isochronal annealing (30 min) at different temperatures for the Russian RPV steels 15Kh2MFA and 15Kh2NMFA. The calibration constant was held in each case on 0.0468 and the statistical error on 0.04%.

irradiated, Q228, X132: non-irradiated). The fifth and sixth steel samples, irradiated (73W) and non-irradiated (732W) are Linde 0124 weld metal. With the aim of comparing western types of RPV steels to eastern ones, Russian 15Kh2MFA RPV steel was studied as well (YA). This second generation Cr–Mo–V type of RPV steel has been commercially used in VVER-440 nuclear reactors since the seventies. The elemental composition and thickness of the investigated specimens, as well as their received treatments are given in Table 2.

Samples have been irradiated for about eight weeks up to a nominal fluence of $\phi = 5 \times 10^{19}$ n/cm^2 (E_n>1 MeV) in the CALLISTO PWR irradiation rig of the BR2 research reactor at the Belgian Nuclear Research Centre (SCK-CEN Mol, Belgium). Isochronal annea-

Table 2
RPV steel samples (Steel type, treatment, concentration of the main alloying elements and thickness are given. Selected samples have been irradiated at 290°C upto a fluence of 5×10^{19} n/cm^2 ($E_n > 1$ MeV).)

Samples			Composition (wt%)							Thickness (μm)
Sample code	Steel type	Treatment	C	Cr	Cu	Mn	Mo	Ni	Si	
JRQ-Q228	A533B Cl. 1	As-received	0.18	0.13	0.14	1.37	0.50	0.82	0.24	37
JRQ-JRQ616	A533B Cl. 1	Irradiated	0.18	0.13	0.14	1.37	0.50	0.82	0.24	62
HSST03-X132	A533B Cl. 1	As-received	0.21	0.10	0.11	1.43	0.51	0.62	0.23	39
HSST03-X51	A533B Cl. 1	Irradiated	0.21	0.10	0.11	1.43	0.51	0.62	0.23	69
73W	Linde 0124	Irradiated	0.10	0.25	0.31	1.56	0.58	0.60	0.45	41
732W	Linde 0124	As-received	0.10	0.25	0.31	1.56	0.58	0.60	0.45	40
YA	15Kh2MFA	As-received	0.14	2.93	0.11	0.40	0.72	0.14	0.24	40

lings of the chosen specimens (range of temperatures: 20–1000°C, step 50°C) were performed in a vacuum better than 3×10^{-3} Pa. Samples were annealed for 30 minutes at each temperature and afterwards cooled down in vacuum to RT using 'low-stress cooling speed' (100°C/h).

In the first stage special attention went to the temperature region up to 700°C. At higher temperatures a new additional singlet component (isomer shift of about −0.298 mm/s) is clearly observable. Its presence can be explained as a paramagnetic austenite formation, which is due to structure changes from bcc to fcc starting at about 720°C. In case of Russian 15Kh2MFA steel, this singlet was observed beyond 800°C.

It can be concluded from this part of the study that in general the thermal treatment, the irradiation and the post-irradiation heat treatment do not drastically affect the Mössbauer parameters. Currently, some small differences observed for the hyperfine fields and fractional areas of the sextets are further examined in some detail; however, the changes are almost within the range of statistical errors (±0.1 T). Results relevant to the comparison between irradiated and non-irradiated RPV steel specimens are presented in Table 3. The influence of isochronal annealing and equivalent post-irradiation heat treatment on the change of MS parameters of IAEA reference quality RPV-steel (JRQ) is shown in Fig. 6.

Only few studies, indicating that MS is a potentially interesting tool to investigate the microstructural aspects of irradiation embrittlement of RPV steels, have been performed so far [9,20]. For this reason it was decided to investigate three RPV steel samples with slightly different chemical compositions to determine the applicability of the Mössbauer effect to the problem of RPV steel embrittlement. The results show that the distribution analysis of the MS enables to distinguish between the different steel types. Small differences in carbon concentration between western base (JRQ) and weld (73W) metal is reflected in the small area fraction of the cementite doublet for the weld metal. Differences between eastern and western type RPV steels are reflected in the overall shape of the derived H_{hf}-DP. The larger fraction of the 'perturbed' area for the eastern steel, the differences in H_{hf} and δ values and the absence of a carbide doublet sub-spectrum are all due to the fact that the overall alloy-element concentration (especially for Cr and V) for the eastern steel is larger than for western-type steels [19,20].

Notwithstanding these encouraging results, a lot of work remains to be done. Additional experiments on a number of samples of different composition, irradiated as well as non-irradiated, have to be performed to gain more insight in the exact nature of the relationship that different alloy elements have with the relevant

Table 3
Relevant RT Mössbauer spectroscopy parameters of irradiated and non-irradiated western-type RPV steels. ($H_{hf,i}$ are the maximum-probability hyperfine fields derived from the H_{hf}-distribution profiles and S_i the corresponding area fraction. The area S_3 belongs to the doublet fraction.)

Type of RPV steel	Treatment	H_{hf1} (T)	H_{hf2} (T)	S_1 (%)	S_2 (%)	S_3 (%)
JRQ steel plate 16.616 (A533B Cl. 1)	As-received	33.1	30.5	81.6	15.6	2.8
	Irradiated	33.1	30.5	80.6	16.4	3.0
HSST03 (A533B Cl. 1)	As-received	33.2	30.5	79.1	18.3	2.6
	Irradiated	33.1	30.4	77.5	19.6	2.9
Linde 0124 weld	As-received	33.1	30.5	80.4	18.2	1.4
	Irradiated	33.1	30.4	80.0	18.2	1.8

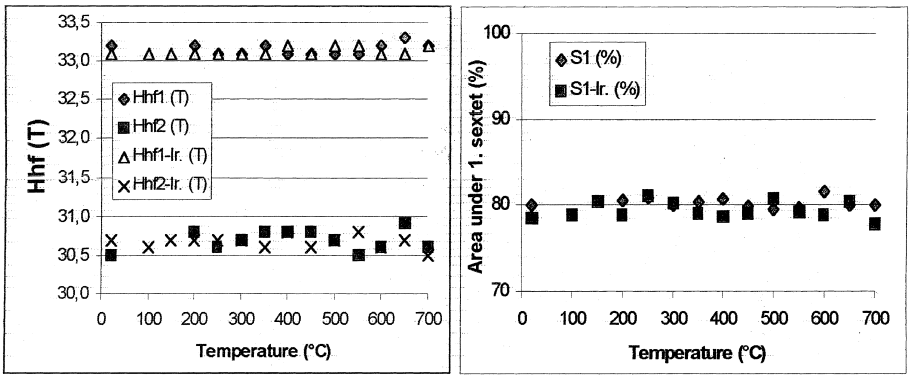

Fig. 6. Influence of isochronal annealing and equivalent post-irradiation heat treatment on the change of Mössbauer spectroscopy parameters of the IAEA reference quality RPV steel (JRQ).

Mössbauer parameters, such as area fractions, isomer shifts and maximum-probability hyperfine-field values.

4. ILEEMS applied to thermally treated Russian RPV steels

The integral low-energy electron MS (ILEEMS) is known to be sensitive only to a thin surface layer of a few nanometers. Specimens in the form of small disks (5 mm diameter, thickness of about 0.8 mm) were polished to the condition 'like mirror' and measured in a high-vacuum ($\simeq 10^{-4}$ Pa) chamber containing a channeltron electron detector. By applying a positive bias of 200 V to the channeltron cathode, it was found possible to detect the low-energy electrons with a reasonable efficiency. The same model as for the transmission MS was used for fitting the ILEEMS spectra. The line width of the *unperturbed* component was fixed at a value of 0.23 mm/s.

ILEEMS was applied on 15Kh2MFA (YT) and 15Kh2NMFA (XT) steels. The chemical composition and preparing technology of used specimens is identical with composition of YTA and XTA specimens shown in Table 1. These HAZ specimens were prepared especially for TEM measurements (reported in Section 5.2).

The ILEEMS results (see Table 4) indicate slight but significant changes in the areas S_1, S_2, S_3 beneath the sextets and basically confirm the transmission MS measurements performed on the 15Kh2MFA specimens. A small gradual decrease in S_3 (which refers to two or more alloying atoms in the nearest neighbourhood) with increasing annealing temperature is probably due to the release of some of the alloying elements as a result of the higher temperature and the precipitation of these elements as carbides or other non-magnetic compounds (see Fig. 7, where results from transmission MS are shown). Nevertheless the area S_2 of the second sextet (*perturbed* component) in dependence on Hollomon–Jaffe parameter could be correlated with the hardness curve. Basically, it is in agreement with our hypothesis about physical explanation of this MS components.

The results further confirm the ability of ILEEMS to detect changes in the surface microstructure due to different thermal treatments.

Table 4
Relevant integral low-energy electron Mössbauer spectroscopy parameters for thermally treated Russian RPV steels (at RT). (The 3-sextets fit, line width of the most pronounced component fixed at 0.23 mm/s, other widths and A1/A3, A2/A3 ratios coupled together.)

Types of RPV-steel	Sample	M par.	$H_{hf,1}$ (T)	$H_{hf,2}$ (T)	$H_{hf,3}$ (T)	δ_1 (mm/s)	$\delta_{2,3}$ (mm/s)	Γ_1 (mm/s)	$\Gamma_{2,3}$ (mm/s)	S_1 (%)	S_2 (%)	S_3 (%)	Hardness
15Kh2MFA	yt35	14640	33.5	31.4	28.3	0.003	−0.009	0.23	0.296	51.7	39.1	9.2	354.9
15Kh2MFA	yt38	16240	33.4	31.3	28.6	0.004	−0.001	0.23	0.348	50.2	40.9	8.9	386.6
15Kh2MFA	yt44	16805	33.4	30.8	28.5	0.001	−0.008	0.23	0.388	46.9	42.1	11.0	392.7
15Kh2MFA	yt51	17490	33.5	31.1	27.0	0.004	−0.002	0.23	0.296	55.2	37.4	7.4	395.6
15Kh2MFA	yt61	19860	33.4	30.7	28.5	0.003	−0.004	0.23	0.322	56.8	36.8	6.4	265.7
15Kh2MFA	yt62	20850	33.4	30.7	28.5	0.000	0.008	0.23	0.331	56.4	35.4	8.2	203.8
15Kh2NMFA	xt2	14070	33.4	31.0	28.4	0.005	−0.001	0.23	0.330	56.0	37.3	6.65	394.1
15Kh2NMFA	xt5	15460	33.4	31.1	28.0	0.005	0.002	0.23	0.349	56.0	37.3	6.7	414.6
15Kh2NMFA	xt14	17920	33.4	31.2	28.0	−0.003	−0.008	0.23	0.298	52.2	39.5	8.2	339.4
15Kh2NMFA	xt30	20850	33.3	30.6	28.6	0.003	0.001	0.23	0.281	69.1	27.8	3.1	201.9

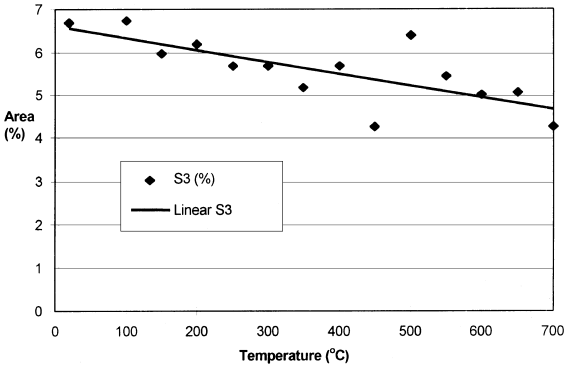

Fig. 7. Areas under the third sextet of MS spectra obtained from isochronal annealing experiment (15Kh2MFA specimen).

5. TEM performed on selected Russian RPV steel specimens

5.1. RPV steels 15Kh2MFA and 15Kh2NMFA from the metallurgical point of view

The 15Kh2MFA and 15Kh2NMFA steels belong to the low alloyed steels, whose structure of the heat affected zone (HAZ) of welded joint consists of an acicular mixture of martensite, self-tempered martensite and bainite depending on the cooling rate. It is well-known that the martensitic structure (or the martensitic–bainitic structure) can be tempered in such a manner that the resultant condition will provide sufficient strength (hardness) and toughness. In alloyed steels there also occurs a secondary hardening with the carbides of alloying elements. The effect of secondary alloying can be dependent on type and content of alloying elements, combined with the hardness drop due to martensite decomposition.

A certain role is played here also by the structure condition, mainly when it does not consist purely of martensite. Though cementite (Fe_3C) is already present in the self-tempered martensite and bainite, the carbides of the alloying elements have not precipitated yet.

In spite of the fact that the iron affinity to carbon is lower than that of other carbide-forming elements (Cr, Mo, V, Ti, etc.) at tempering, the cementite is first precipitated and just after attaining the temperature of 500–600°C the carbides of other elements are precipitated, or the content of M_3C carbides is gradually decreased.

In vanadium-containing steels (for example 1/2Cr1/2Mo1/4V, 1Cr1/4V, 3Cr1Mo1/4V, 1Cr1Mo3/4V) vanadium carbide (VC) is precipitated during tempering, since the solubility of this carbide is higher than that of cementite or chromium and molybdenum carbides. VC is precipitated in the form of small plates (diameter below 5 nm and thickness below 1 nm). This phenomenon takes place in the temperature range from 500°C to 650°C, which results in secondary hardening of the steel [21,22].

Precipitation hardening of weld joint HAZ at annealing seems to be one of the reasons contributing to reheat crack formation. Both steels (15Kh2MFA and 15Kh2NMFA) differ from each other by the content of carbide-forming elements, which affects the course of secondary hardening. To solve the practical questions, concerning the selection of optimum heat treatment parameters of weldments of the above-mentioned steels it is advisable to know the thermal and time dependences of welded joint hardening.

5.2. Experiments

For the hardness measurement and the study of structural transformation the steels with compositions given in Table 1 were used (HAZ samples XTA and YTA). The aim of the experiments was to map the course of hardness variations due to structure tempering and precipitation of alloy carbides. At temperatures above 400°C the structural transformation can occur even during the heating phase. Therefore an equivalent dwell time was considered, which would include not only the total dwelling, but also the heating time. The equivalent heating time was calculated on the basis of the following relationship

$$t_h = \frac{T}{2.3k(20 - \log k)},$$

where T is the annealing temperature in K, k the heating rate in K/h. The calculated heating time (t_h) is given in seconds.

The following temperatures were selected for annealing: 500°C, 580°C, 650°C, 720°C; equivalent dwell times: 30 s, 1, 5, 30 min; 1, 10, 20, 50 h. A furnace ESA type K 59 was used for heat treatment. After an appropriate dwell time at the annealing temperature the specimens were water cooled.

5.3. Results

The Vickers hardness after weld thermal cycle of both steels was as follows:

15Kh2MFA: 356 HV10

15Kh2NMFA: 396 HV10.

By comparing the hardness course of both studied steels we found out that the precipitation hardening of the 15Kh2NMFA steel takes place faster than that of the 15Kh2MFA steel. This means that shorter dwell times are sufficient to complete the precipitation re-ageing and thus, acceptable strength and plastic properties can be attained. The curves of hardening kinetics at different temperatures were calculated to a temperature-time parameter, which is also called the Holloman–Jaffe parameter (Fig. 8):

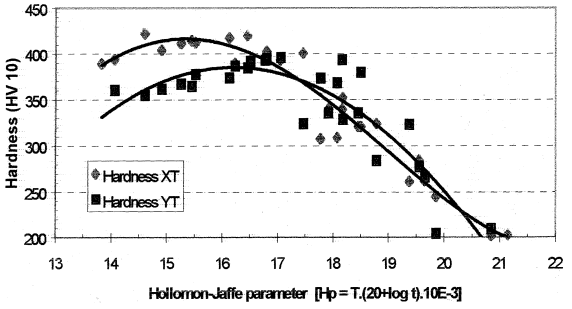

Fig. 8. Dependence of hardness of the simulated HAZ of 15Kh2MFA and 15Kh2NMFA steels on the Hollomon-Jaffe's parameter H_p.

$$H_p = T(20 + \log t) \times 10^{-3}.$$

Such interpretation is advantageous in the prediction of the expected hardness change at an arbitrary selection of temperature and dwell time, or for determining the heat treatment parameters at the conditions of assuring the desired final hardness of a welded joint.

5.4. Microstructural analysis

During the heat treatment a different level of structure tempering from the initial condition takes place, depending on the temperature and time of tempering. In principle, a diverse degree of decomposition of the bainitic-martensitic mixture is concerned. Moreover, a secondary hardening by carbide-forming alloying elements also occurs. The structures from the initial condition up to a significant hardness drop at 650°C for 20 h dwell time were gradually analysed.

The initial condition of the microstructure of both steels can be characterised as an acicular mixture of martensite, self-tempered martensite and bainite. The structure of carbides (M_3C) was evaluated on the basis of diffraction spectra (see Table 5. For each type or size of carbides 10 measurements as minimum was performed). The structural and chemical analysis at the condition 650°C/1 min was similar, however the carbide phase on the grain boundaries became more pronounced.

Condition 650°C/5 min – 15Kh2MFA steel. The carbides on the grain boundaries contain already a higher chromium level. The initial Fe_3C carbide in the matrix contains only a minimum amount of chromium. This process is even slower in the 15Kh2NMFA steel. The carbide type M_3C is structurally stable. More significant morphological changes were not encountered, which follows also from the dimensions given in Table 5.

Condition 650°C/30 min – 15Kh2MFA steel. On the boundary in M_3C carbide the chromium content is monotonously increased (locally even at 20%). The chromium traces in the matrix are also fully evident. In the 15Kh2NMFA steel the enrichment of chromium carbides on the grain boundaries became more pronounced (Table 5). In addition also Mo appeared. In the matrix, beside the iron containing carbides also the carbides containing Cr or those with chromium contents up to 6% also occurred. The structure of the carbides in both steels remained of the M_3C type. A significant fact was the indication of a fine precipitate of VC in the matrix. It can be said that the precipitation of a non-coherent VC resulted in a hardness drop by 50 HV units (Fig. 8).

Condition 650°C/1 h – the results of the analysis are again given in Table 5. With both steels a hardness drop is evident, however, it is not so significant with the 15Kh2MFA steel as with the 15Kh2NMFA steel. Regarding the chemical composition and structure of carbides, more pronounced changes in both steels have been observed. On the grain boundary, there are carbides containing Fe (up to 80 weight %) and Cr (up to 20 wt%) with the structure type M_3C and carbides containing already all carbide-forming elements with Cr prevalence (up to 50 wt%) with the structure type M_7C_3. Also a simultaneous diffraction of both structures occurred, however, regarding the carbide clusters it cannot be unanimously stated whether it is a doubled diffraction or just in situ transformation of the M_3C–M_7C_3 carbide. On a carbon extraction replica from the15Kh2MFA steel structure the VC was not identified yet.

Condition 650°C/10 h – is characterised with a hardness drop for both steels into the range of remarkable overageing of steel. The M_7C_3 carbide starts to prevail with an appropriate composition, where all carbide-forming elements are included. A sufficient amount of M_3C carbide is still present, where only Fe and Cr are represented, or also other carbide-forming elements, however not in such an amount. From the morphological viewpoint it is also evident that the cementite particles are loosing their compact shape. In the 15Kh2MFA steel structure MC carbides were identified, which are partially enriched with Mo and Cr.

Condition 650°C/20 h – corresponds to the characteristic of the previous stage. In the 15Kh2MFA steel only the carbides with the M_7C_3 and MC structures were identified. In the 15Kh2NMFA steel there are still M_3C carbide residues. The carbides are in average much coarser. Fine carbides of the MC type can be identified already at smaller magnification (Fig. 9). This characteristic is in principle valid for both steels.

5.5. Discussion

The curve of the hardness dependence on temperature and time on annealing exerts a character typical for the precipitation hardening of steels. As evident the

Table 5
Carbides identified in the HAZ specimens of the RPV-steels 15Kh2MFA and 15Kh2NMFA

Treatment	Location	Type of carbide	Chemical composition – semi-equivalent microanalysis (wt%)									
			15Kh2MFA					15Kh2NMFA				
			Size (nm)	Fe	Cr	Mo	V	Size (nm)	Fe	Cr	Mo	V
Simulated HAZ	Border	M_3C	20–60	Pure Fe				10–50	Pure Fe			
	Matrix	M_3C	20–60	Pure Fe				25–40	Pure Fe			
			50–200	Sometimes Cr traces				100–200				
650°C – 5 min	Border	M_3C	20–60	>90	<10	–	–	15–50	Pure Fe			
			50–300	>90	<10	–	–	50–180	Sometimes Cr traces			
	Matrix	M_3C	25–100	Pure Fe				25–70	Pure Fe			
			70–300	Sometimes Cr traces				60–300				
650°C – 30 min	Border	M_3C	20–80	>80	<20	–	–	40–100	<80	<20	<3	–
			50–350	>80	<20	–	–	60–300	<80	<20	<3	–
	Matrix	M_3C	50–100	Pure Fe				20–100	Pure Fe			
			70–300	Sometimes Cr traces				60–400	Cr traces (up to 6%)			
	Matrix	MC	–	–	–	–	–	<10	–	–	–	100
650°C – 1 h	Border	M_3C	20–40	<80	<20	–	–	30–70	<80	<20	–	–
			100–200	<80	<20	–	–	60–390	<80	<20	–	–
	Matrix	M_3C	30–100	<85	<25	–	–	10–70	<90	<20	Traces	–
			40–270	<85	<25	–	–	80–300	<90	<20	Traces	–
	Border	M_7C	20–60	<40	<50	<10	<3	20–80	<41	<52	<5	<2
			80–170	<40	<50	<10	<3	90–300	<41	<52	<5	<2
	Matrix	MC	–	–	–	–	–	–	–	–	–	100
650°C – 10 h	Matrix	M_7C_3	20–60	<30	<60	<10	<4	30–100	<40	<50	<9	<2
			80–200	<30	<60	<10	<4	110–300	<40	<50	<9	<2
		M_3C	10–30	50	50	–	–	20–90	<70	<35	<3	<1
			20–50	50	50	–	–	80–150	<70	<35	<3	<1
		M_3C	40–100	<80	<20	<6	<2					
			60–250	<80	<20	<6	<2					
		MC	<10	V with Mo and Cr traces								
650°C – 20 h	Matrix	M_7C_3	30–240	<34	<57	<11	<6	30–200	<43	<54	<28	<1
		M_3C	–					10–70	<70	<30	<3	<1
								50–120	<70	<30	<3	<1
		MC		V with Mo and Cr traces				–				

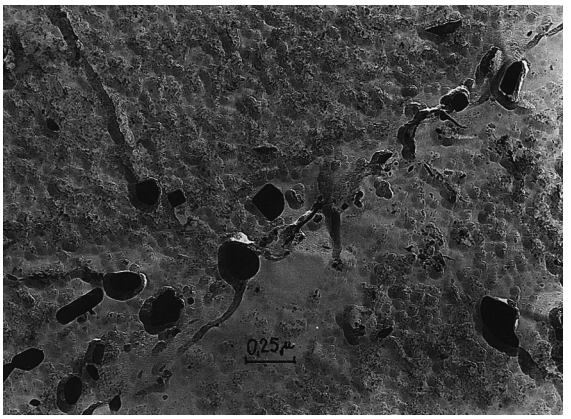

Fig. 9. Coagulation of carbides after heat treatment 650°C/20 h (CR).

hardness changes of the initial condition (simulated HAZ) considerable depend on the temperature:

With increasing temperature, the time necessary for achieving maximum hardness is reduced and the structure of the superheated section of the HAZ is softened considerably faster. In principle, this character corresponds to the results, which were measured on the quenched samples [22]. When observing the course of hardness curves of both studied steels it will be shown that the internal of dispersion hardening of the 15Kh2NMFA steel is shifted to the to the side of shorter dwell times.

To elucidate the effect of the hardening process, the changes of the carbide phase in the matrix were studied. In the initial condition, the simulated HAZ contains only the carbide type M_3C, whose metallic M element was formed only by Fe. The occurrence of carbides on the grain boundaries was limited. At heat treatment under the initial condition a gradual enrichment of M_3C carbides with chromium occurred. That happened to a greater extend on the grain boundaries than in the matrix and it was faster in the 15Kh2MFA steel than in the 15Kh2NMFA steel. The carbide type M_7C_3 was identified only after one hour of dwell time at 650°C. With M_7C_3 carbides it was not unanimously ascertained, whether an in situ formation in place of M_3C carbide was concerned, or a separate formation, or whether both processes contributed to its formation.

A significant hardness drop on the curves of hardening kinetics can be clearly connected with the identification of the already non-coherent carbide type MC. In the 15Kh2NMFA steel the non-coherent MC carbide was identified already after 30 min which contained only V and in the 15Kh2MFA steel after ten hours and that contained beside V also the traces of Cr and Mo. This means that the coherent VC (MC) caused the secondary hardening of the simulated HAZ.

Regarding the time changes of the carbide phase it can be stated that the level of the M_7C_3 carbide continually increases to the detriment of M_3C. The results of the analysis of the precipitation kinetics of the carbide phase of the simulated HAZ structure are in a good agreement with the results which were measured during precipitation of carbides in the 15Kh2MFA and 15Kh2NMFA steels after quenching [23,24].

It is still necessary to clarify why the 15Kh2NMFA steel attains a higher hardness after the HAZ simulation and why it attains faster a maximum of secondary hardening. The effect of carbide-forming elements on the course of tempering is pronounced especially at elevated temperatures, which is related mainly to their diffusivity. The activation energy of diffusion of the individual carbide-forming elements is different and therefore diverse steels can attain the hardness maximum at different temperatures and hold times. The formation of alloy carbides takes place usually in temperature range 400°C – A_{c1}. Below this temperature the formation of alloy carbides does not occur, since the alloying elements cannot diffuse sufficiently fast to enable the nucleation of alloy carbides. Vanadium has a higher affinity to carbon than chromium and molybdenum. At the same time the precipitation of VC takes place at higher temperatures at a slower rate than the precipitation of chromium carbides.

From the viewpoint of the alloying element contents, the 15Kh2MFA steel (C = 0.14 wt%, Cr = 2.22 wt%, Mo = 0.72 wt%, V = 0.31 wt%) contains more than the 15Kh2NMFA steel (C = 0.18 wt%, Cr = 2.22 wt%, Mo = 0.62 wt%, V = 0.08 wt%) which moreover contains also Ni. Nickel is an element known for increasing the austenite stability and thus subsequently also by the shift of martensitic transformation. This is evident also from the diagrams of the anisothermal austenite decomposition (measured by the in situ method) for both steels [25], where the temperature of begin and end of the individual transformation is lower for the nickel containing steel than for the nickel-free steel. This results in a higher final hardness due to totally larger transformation hardening and lower proportion of self-tempered martensite. Nickel also improves the solubility of interstitial elements.

It is necessary to explain the faster precipitation of VC in nickel containing steels. A simple explanation is offered on comparison the carbon concentration with the carbide-forming elements, or with vanadium itself. The 15Kh2MFA steel contains 0.65 at.% C, 3.12 at.% Cr, 0.41 at.% Mo, 0.34 at.% V, which represents the proportion M:C = 6:1 or V:C = 0.5:1. The 15Kh2NMFA steel contains 0.83 at.% C, 2.37 at.% Cr, 0.35 at.% Mo, 0.1 at.% V, which represents the proportion M:C = 3.4:1 or V:C = 0.12:1. Since the V:C value is approximately four times higher for the 15Kh2NMFA steel, there are more advantageous

conditions for carbide precipitation in this steel. Its role is significant also by the fine dispersion of phases due to lower temperatures of the appropriate phase transformation.

6. Conclusion

The methods as PAS, LT, DB, MS, ILEEMS and TEM were applied to the RPV steel investigation. In total eight different PRV steels were studied using some of these methods with the aim to extract some novel information about the microstructural changes caused by thermal, irradiation and post-irradiation heat treatments.

Clear differences between western and eastern types of commercially used RPV steels were observed, compared and discussed using PAS and MS. According to the results from the PAS mean-lifetime analyses, the observable differences in the values and behaviours of successive annealing curves are caused not only by different chemical compositions, but also due to different preparation technologies of the RPV steels. This fact was confirmed for the 15Kh2MFA steel, from which the base material and simulated HAZ were studied simultaneously.

Changes in the steel microstructure due to the phase transition from bcc to fcc, starting at about 725°C, were observed for all western types of RPV steels using PAS. In case of Russian RPV steels, this phase transition was not observed below 800°C. The same is reflected in the MS, where the presence of the paramagnetic austenite was clearly detected at 750°C in western batches of steels and at 800–850°C in Russians steels.

The Mössbauer study shows that the distribution analyses of the MS enables to distinguish between the different steel types. Small differences in carbon concentration between western base (JRQ) and weld (73W) metal is reflected in the small area fraction of the cementite doublet for the weld metal. Differences between eastern and western type RPV steels are apparent in the overall shape of the derived H_{hf}-DP. The larger fraction of the perturbed area for the eastern steel, the differences in H_{hf} and δ values, and the absence of a carbide doublet sub-spectrum are all due to the fact that the overall alloy-element concentration (especially Cr and V) for the eastern steel is larger than for western-type steels.

From Mössbauer measurements performed on the western type of RPV steels A533B Cl.1 (JRQ, HSST03) and Linde 0124 weld (73W), we can conclude that thermal treatment (up to 700°C), irradiation (up to $\phi = 5.10^{19}$ n/cm^2 ($E_n > 1$ MeV)) and post-irradiation heat treatment did not affect MS substantially.

On the other hand, the first MS measurements performed on the Russian RPV steel 15Kh2MFA, irradiated with a comparable neutron fluence ($\phi = 6.7 \times 10^{19}$ n/cm^2, $E_n > 0.5$ MeV) in the framework of the 'Surveillance Specimen Program', revealed recently observable changes in the relevant parameters of the MS [26].

RPV embrittlement (limiting factor in the lifetime of vessels of today's NPP) is a more pronounced problem in eastern (Russian) types of nuclear reactors (VVER-440). It is due to the narrower gap between the outside surface of the core barrel and the inside surface of the RPV than in western RPVs. The neutron flux and consequently the neutron fluence on the RPV wall is generally higher on VVER-440 type reactors than in other equivalent types. This influence of neutron flux (even neutrons of energy over 0.1 MeV) on the RPV embrittlement is much more impressive than contributions from a coolant temperature or an operational pressure in the primary circuit. Therefore, PAS, MS and TEM measurements on several RPV specimens irradiated in the NPP Bohunice (Slovakia) during their one-, two-, three- and five-year stays into the operating nuclear reactor, started in the framework of the 'Extended Surveillance Specimen Program' (1994) are in progress. New additional information about microstructural changes in thermally and irradiation-treated RPV materials are expected in the next years (neutron diffraction should be included for the study in the near future).

It was confirmed that HAZ is the most sensitive place for thermal and neutron embrittlement in the reactor. PAS LT measurements on the successively annealed HAZ specimens (XTA, YTA) have shown the rapid increase in the vacancy-type defect formation in the temperature region 525–600°C. Therefore these specimens were studied using TEM in more detail.

According to the TEM measurements, the time dependences of hardening of the simulated HAZ of 15Kh2MFA and 15Kh2NMFA steels were plotted for the temperatures of 500, 580, 650 and 720°C. The time corresponding to the hardness maximum in the dependences HV $10 = f(t)$ for 650°C annealing temperature is shorter than the time after elapsing of which the non-coherent particles of MC carbide were observed. This corresponds with the picture of precipitation hardening. It was shown that the kinetics of MC carbide precipitation depends on the chemical composition of the steel.

The kinetics of carbide phase precipitation were studied from the viewpoint of chemical composition and structure. It was shown that in the simulated HAZ, carbides of type M_3C, M_7C_3 and MC are formed during annealing (650°C). Their chemical composition depends on the dwell time at the annealing temperature. It was found out that in 15Kh2MFA and 15Kh2NMFA steels, precipitation hardening at temperatures above 580°C occurs already after very short dwell time (below 1 h). This finding is essential from the viewpoint of assessment of steel resistance against formation of reheat or underclad cracks.

According to the obtained results, it is possible to conclude that the used test methods can produce progress in the microstructural study of RPV steels and in the optimisation of the temperature-time regime for the regenerative post-irradiation thermal treatment of RPVs.

Acknowledgements

The authors would like to thank NATO (V. Slugeň Research Fellowship – 1996), IAEA (Research contract 9001/RBF), SGA (Grant No. 1/4286/97) and NFWO (Grant No. 32001493) for support.

References

[1] W.J. Phythian, C.A. English, J. Nucl. Mater. 205 (1993) 162.
[2] G. Brauer, L. Liszkay, B. Molnar, R. Krause, Nucl. Eng. Design 127 (1991) 47.
[3] R. Pareja, N. De Diego, R.M. De Le Cruz, J. Del Rio, Nucl. Technol. 104 (1993) 52.
[4] C. LopesGil, A.P. De Lima, N. Ayres De Campos, J.V. Fernandez, G. Kögel, P. Sperr, W. Triftshäuser, D. Pachur, J. Nucl. Mater. 161 (1989) 1.
[5] Z.P. Abdurasulev, P.U. Arifov, N.I. Artjumov, Methods for Positron Annihilation Diagnostics and Evaluation of Spectra, FAN Taskent, 1985 (in Russian).
[6] P. Hautojärvi, Positrons in Solids, Springer, Berlin, 1979.
[7] M. Valo, R. Krause, K. Saarinen, P. Hautojarvi, R. Hawthorne, ASTM STP 1125, Stoller, Philadelphia, 1992.
[8] F. Bečvár, Y. Jirásková, E. Keilová, J. Kočík, L. Lešták, I. Procházka, B. Sedlák, M. Šob, Mater. Sci. Forum 105–110 (1992) 901.
[9] G. Brauer, W. Matz, L. Liszkay, B. Molnar, R. Krause, Mater. Sci. Forum 97–99 (1992) 379.
[10] G. Brauer, Mater. Sci. Forum 175–78 (1995) 303.
[11] L. Cohen, Application of Mössbauer Spectroscopy, vol. II, Academic Press, New York, 1980.
[12] G. Brauer, W. Matz, C. Fetzer, Hyperf. Interact. 56 (1990) 1563.
[13] A.D. Amaev, Yu.G. Dragunov, A.M. Kryukov, L.M. Lebedev, M.A. Sokolov, Investigation of irradiation embrittlement of reactor VVER-440 vessel materials, in: IAEA Specialists Meeting Proceedings, Plzen, 1986.
[14] T. Šmída, V. Magula, Zváranie (in Slovak) 37 (1) (1988) 34.
[15] P. Kirkegaard, N. Pedersen, M. Eldrup, PATFIT 88 – A data processing system for positron annihilation Spectra on Mainframe and Personal Computers, Risõ, M-2740, 1989.
[16] A. Shukla, M. Peter, L. Hoffman, Nucl. Instrum. and Meth. A335 (1993) 310.
[17] M.A. Monge, J. del Rio, J. Phys.: Condens. Matter 6 (1994).
[18] N. Djourelov, M. Misheva, J. Phys.: Condens. Matter 8 (1996).
[19] P. De Bakker, V. Slugeň, E. De Grave, E. Van Walle, A. Fabry, Hyperf. Interact. 110 (1997) 11.
[20] J. Haščík, J. Lipka, L. Kupča, V. Slugeň, M. Miglierini, R. Gröne, I. Tóth, K. Vitázek, Acta Phys. Slovaca 45 (1995) 37.
[21] R.W.K. Honeycombe, Steels-Microstructure and Properties, Edward Arnold, London, 1981.
[22] V. Magula, Research Report No.:ZA 01-123-811-03/16380/21, VÚZ Bratislava, October 1987 (in Slovak).
[23] J. Janovec, V. Magula, Kov. Mater. 26 (in Slovak) (6) (1988) 141.
[24] M.M. Sandovniuskij, Avtomaticeskaja svarka (in Russian) (10) (1982) 322.
[25] V. Magula, J. Janovec, Ironmaking Steelmaking 21 (1994) 223.
[26] V. Slugeň, IAEA Final Research Report 9001/RBF, KJFT FEI STU Bratislava, 1998.